



Deposited via The University of Sheffield.

White Rose Research Online URL for this paper:

<https://eprints.whiterose.ac.uk/id/eprint/165132/>

Version: Accepted Version

Article:

Nkiaka, E., Nawaz, R. and Lovett, J.C. (2018) Assessing the reliability and uncertainties of projected changes in precipitation and temperature in Coupled Model Intercomparison Project phase 5 models over the Lake Chad basin. *International Journal of Climatology*, 38 (14). pp. 5136-5152. ISSN: 0899-8418

<https://doi.org/10.1002/joc.5717>

This is the peer reviewed version of the following article: Nkiaka, E, Nawaz, R, Lovett, JC. Assessing the reliability and uncertainties of projected changes in precipitation and temperature in Coupled Model Intercomparison Project phase 5 models over the Lake Chad basin. *Int J Climatol*. 2018; 38: 5136– 5152, which has been published in final form at <https://doi.org/10.1002/joc.5717>. This article may be used for non-commercial purposes in accordance with Wiley Terms and Conditions for Use of Self-Archived Versions.

Reuse

Items deposited in White Rose Research Online are protected by copyright, with all rights reserved unless indicated otherwise. They may be downloaded and/or printed for private study, or other acts as permitted by national copyright laws. The publisher or other rights holders may allow further reproduction and re-use of the full text version. This is indicated by the licence information on the White Rose Research Online record for the item.

Takedown

If you consider content in White Rose Research Online to be in breach of UK law, please notify us by emailing eprints@whiterose.ac.uk including the URL of the record and the reason for the withdrawal request.

Assessing the reliability and uncertainties of projected changes in precipitation and temperature in CMIP5 models over the Lake Chad basin

Elias Nkiaka¹, Rizwan Nawaz² and Jon C. Lovett¹

¹School of Geography, University of Leeds.

²Department of Civil & Structural Engineering, University of Sheffield

Correspondence to: Elias Nkiaka (gyenan@leeds.ac.uk)

Abstract

Lake Chad lost more than 80% of its surface area over the past decades as a result of environmental change and climate variability. It is not yet known how climate change will affect water resources availability in the basin over the coming decades. In this study, the Reliability Ensemble Averaging (REA) technique was used to evaluate the performance of CMIP5 models in simulating present-day precipitation and temperature (1980 – 2005); and to quantify the uncertainties in future projections (2050 – 2075) under two Representative Concentration Pathways (RCPs) in the Lake Chad basin (LCB). Analyses were carried out at both annual and seasonal time-scales. Overall, the CMIP5 models simulated precipitation better than temperature in the study area. Although the models were able to simulate the annual precipitation cycle in the basin, most models overestimated precipitation during the dry season and underestimated it during the monsoon season. Future annual basin precipitation is projected to increase by 2.5% and 5% respectively under RCP4.5 and RCP8.5 scenario by the middle of the century by most of the models and most of the model projections are within the REA uncertainty range. Despite the increase in projected annual precipitation in the basin, most models project a decrease in monsoon precipitation under both RCPs. Although the uncertainty range for future precipitation projections for most models lie within the range of natural climate variability, additional analysis are needed for results to be useful for any future planning in the study area.

Keywords: Lake Chad basin, reliability ensemble averaging, uncertainty quantification, CMIP5, climate projections, climate change, simple model averaging

1. Introduction

Climate change is expected to cause major disruptions to the global hydrological cycle as a result of changes in precipitation patterns with the impacts expected to be exacerbated by rising

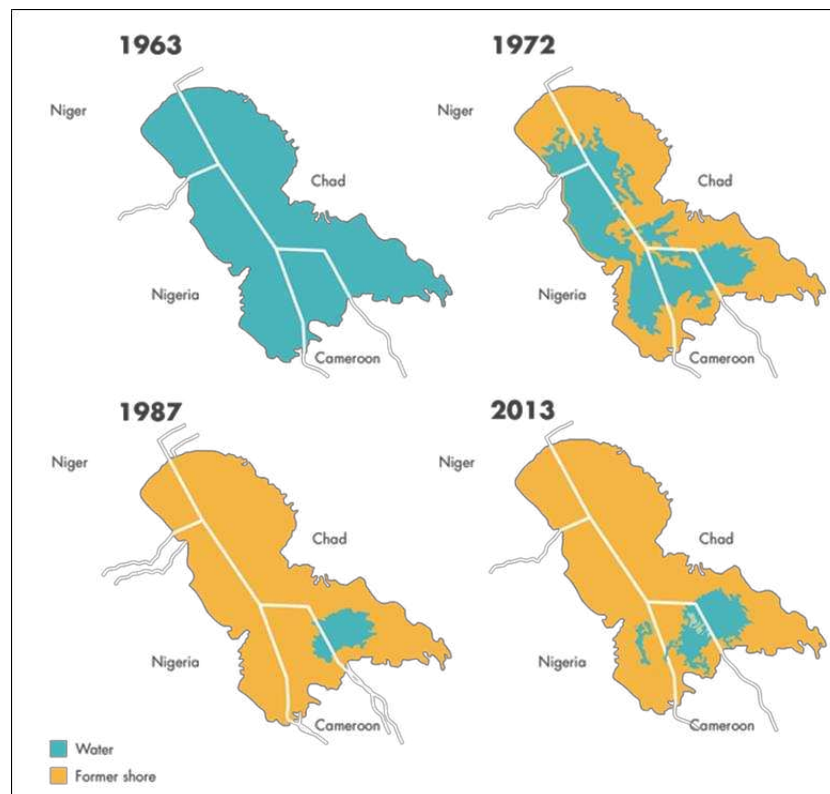
33 global population (Arnell 2004; Trenberth 2011; Gosling and Arnell 2016). For example in some
34 tropical regions like the Sahel, the frequency of storm events has increased by three folds over the
35 past three decades as a result of global warming (Taylor et al. 2017). Therefore, developing future
36 water resources management and planning strategies under anticipated climate change requires the
37 estimation of current and future precipitation magnitude and variability (Wehner 2013). This can be
38 achieved through the application of Global Circulation Models (GCMs) which are used to predict
39 climate change associated with future scenarios of greenhouse gas concentrations (Siam et al. 2013).
40 For these climate models to be used for impact studies, they need to be evaluated against observed
41 data to assess their performance in simulating the present-day climate. Even so, it has been reported
42 that GCM skill in simulating the present-day climate relates very weakly to its ability to simulate
43 projected climate (Knutti et al. 2010).

44 Notwithstanding, different techniques have been applied to evaluate the performance of
45 GCMs in simulating present and future precipitation and temperature changes. These methods range
46 from simple statistical techniques e.g. mean errors, correlations, root-mean-square errors (Akurut et
47 al. 2014) to advanced statistical techniques e.g. volumetric hit index (VHI) (Mehran et al. 2014).
48 Such methods are used to compare model output with observations. The second widely used
49 evaluation method is the diagnostics approach that provide information on the sources of model
50 errors and how to identify processes connected with these errors e.g. analysis of energy and water
51 cycles, and analysis of atmospheric and land processes (Siam et al. 2013). Another approach is the
52 evaluation of GCMs based on their ability to simulate specific atmospheric processes such as the
53 monsoon precipitation in the tropics, ENSO events and other atmospheric processes that influence
54 the climate of a region (Rowell 2013).

55 Despite the various evaluation techniques available, a fundamental problem associated with
56 the application of GCMs is how well they can simulate climate at the regional scale. While GCMs
57 projections may be consistent in terms of global mean changes, they generally disagree on the
58 magnitude, and in many cases the sign, of change at a regional scale, especially precipitation patterns
59 (Meehl et al. 2007). This raises the issue of uncertainty associated with the use of GCMs. Many
60 methods used for evaluating GCMs do not consider the issue of uncertainty inherent in climate
61 models. In fact, there are many sources of uncertainties associated with the use of GCMs including:
62 natural climate variability, variability between and within models and uncertainty caused by the
63 future emissions of greenhouse gases (GHGs). How this uncertainty can be quantified to enhance
64 decision making remains a challenge. It has been recognized that, uncertainty quantification is a

65 critical component in the description and attribution of climate change (Katz et al. 2013). The most
66 popular method used for assessing uncertainties in GCMs projections is the application of large
67 independent multi model ensembles (MMEs) from different modelling groups under different
68 scenarios to determine future climate projections (Tebaldi and Knutti 2007; Knutti et al. 2010).

69 Generally, the approaches available for uncertainty estimation in GCMs are limited in the
70 literature. Despite this limitation, Koutsoyiannis et al. (2007) used a combination of analytical and
71 Monte Carlo methods to determine the uncertainty limits for temperature, precipitation and runoff
72 projections from GCMs for a catchment in Greece. Woldemeskel et al. (2012) developed and tested
73 the square root of error variance (SREV) method for quantifying uncertainty in future precipitation
74 and temperature projections from GCMs at global scale. Min and Hense (2006) applied the Bayesian
75 model averaging (BMA) technique for uncertainty assessment in global mean surface temperature
76 from an ensemble of GCMs projection. Giorgi and Mearns (2002) developed and tested the
77 Reliability Ensemble Averaging (REA) technique for uncertainty estimation in GCMs at regional
78 scale.



79
80
81

Figure 1: Desiccation of Lake Chad 1963 – 2013 (source: UNEP DIVA-GIS)

82 Many models participating in the fifth phase of the Coupled Model Intercomparison Project
83 (CMIP5) (Taylor et al. 2012) have been evaluated across different regions in Africa. For example
84 Akurut et al. (2014) evaluated precipitation estimates from CMIP5 models over the Lake Victoria,
85 Siam et al. (2013) evaluated the performance of CMIP5 models in the Congo and Upper Blue Nile
86 river basins, Biasutti (2013) tested the performance of CMIP5 models on the prediction of Sahel
87 rainfall. Despite these numerous studies in Africa, none of them considered the quantification of
88 GCM uncertainty. Meanwhile, the Lake Chad basin (LCB) remains poorly represented in those
89 studies despite the significant changes that have been observed in the hydrological dynamics of the
90 basin.

91 From 1960 to 2000, Lake Chad, an endorheic lake located in Central Africa experienced one
92 of the most significant and sustained reduction in rainfall recorded anywhere in the world causing
93 the lake area to shrink by more than 80% (Odada et al. 2009) (Figure 1). Despite this remarkable
94 shrinkage, the LCB remains one of the most under-studied basins in Africa in terms of understanding
95 the climate dynamics in the basin and how it will be affected by future climate change. This issue is
96 further exacerbated by inadequate observational records in the region (Nkiaka et al. 2017a). Despite
97 the scarcity in research output, Armitage et al. (2015) used paleo-climate records from the LCB to
98 show that Lake Mega-Chad exerts a strong control on global biogeochemical cycles. Nkiaka et al.
99 (2017b) analyzed past annual and seasonal rainfall in the southern part of the LCB and reported of
100 a general decline in monsoon precipitation over the period 1951 – 2000. However, no study has
101 focused specifically on future precipitation and temperature projections in the LCB using the recent
102 or previous generations of climate models.

103 Even so, results from previous climate models projections for future precipitation in Central
104 Africa have produced contrasting results. Haensler et al. (2013) evaluated an ensemble of CMIP3/5
105 and RCMs in the Central Africa region and concluded that no significant changes in precipitation
106 may be observed in the region by the end of the present century under two representative
107 concentration pathways (RCPs) RCPs 4.5 and 8.5. In a separate study; Aloysius et al. (2016),
108 reported that CMIP5 models were projecting an increase in future precipitation by the end of the
109 present century in the area of their study domain covering the LCB under RCPs 4.5 and 8.5.
110 Meanwhile, using the regional climate model REMO forced by two GCMs (Europe wide
111 Consortium Earth System Model (EC-Earth) and Max-Planck Institute Earth System (MPI-ESM)),
112 Fotso-Nguemo et al. (2017), reported that future precipitation over the area of their study domain
113 covering the LCB will decrease by the end of the present century under RCPs 4.5 and 8.5. Results

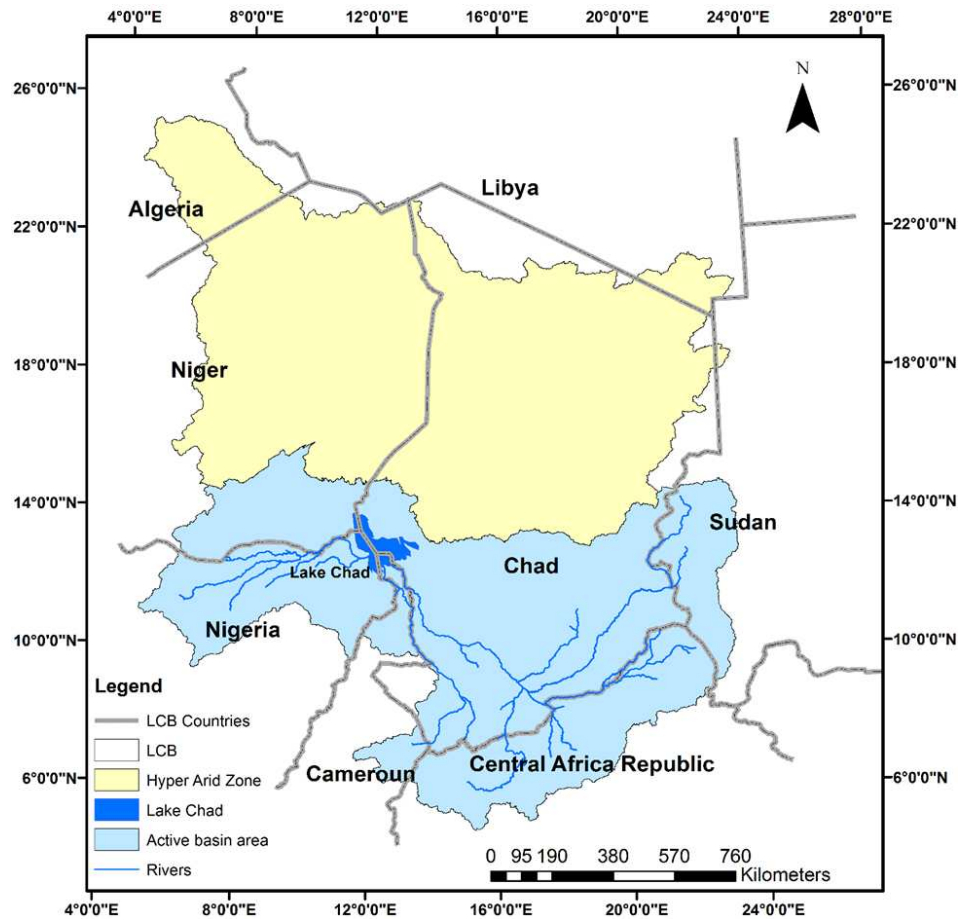
114 from those studies are quite contrasting and cannot be used for any impact studies to enhance
115 adaptation planning in the region, hence the necessity to carry out the present study in the LCB.

116 Although floods have become recurrent in recent years across the LCB causing widespread
117 socio-economic damages, water availability for agriculture, pastoral activities, ecosystem
118 sustainability and contribution as inflow into Lake Chad, is still under threat due to the erratic nature
119 of rainfall. In addition, water resources in the LCB are becoming increasingly vulnerable due to
120 rising population causing tension among water users (Ngatcha 2009). A study by Okpara et al.
121 (2015) has shown that climate-induced water scarcity in the LCB could combine with other human
122 factors such as population increase, poverty and political instability to create a fertile environment
123 for armed conflict. Given the increasing number of refugees in the LCB as a result of “boku haram”
124 terrorist activities in the region (OCHA 2017), climate change could aggravate the current situation
125 resulting in mass migration which could threaten global security. With these myriad of challenges,
126 there is need for research that can enhance our understanding on how precipitation and temperature
127 which determine the availability of water resources will be affected by future climate change in the
128 LCB. This is a crucial knowledge gap in the LCB that this research seeks to fill.

129 The objectives of this study were to: (i) evaluate the ability of CMIP5 models to reproduce
130 the present-day climate conditions in the LCB (1980-2005); (ii) assess the future climate projections
131 for the basin by the middle of century (2050 – 2075) relative to the historical period, and quantify
132 the uncertainties associated with these projections using two representative concentration pathways
133 (RCP4.5 and 8.5); and (iii) evaluate the performance of each ensemble member. This was achieved
134 using the Reliability Ensemble Averaging (REA) technique. The method has been used in previous
135 studies to establish uncertainty limits in GCMs projections (Giorgi and Mearns 2002; Rawlins et al.
136 2012; Miao et al. 2014). At smaller spatial scale, the technique has been used to evaluate CMIP5
137 models by (Rawlins et al. 2012; Sengupta and Rajeevan 2013; Tanveer et al. 2016). The advantages
138 of the REA technique compared to other methods include the fact that the uncertainty range around
139 the simulated changes can be reduced by minimizing the influence of “outlier” or poorly performing
140 models and it also offers the possibility to calculate the uncertainty range around the REA average

141

142



143

144 Figure 2: Lake Chad Basin: Latitudes 5-10 N (sudano), 10-12 N (semi-arid) and 12-16 N (arid)

145 **2. Study area**

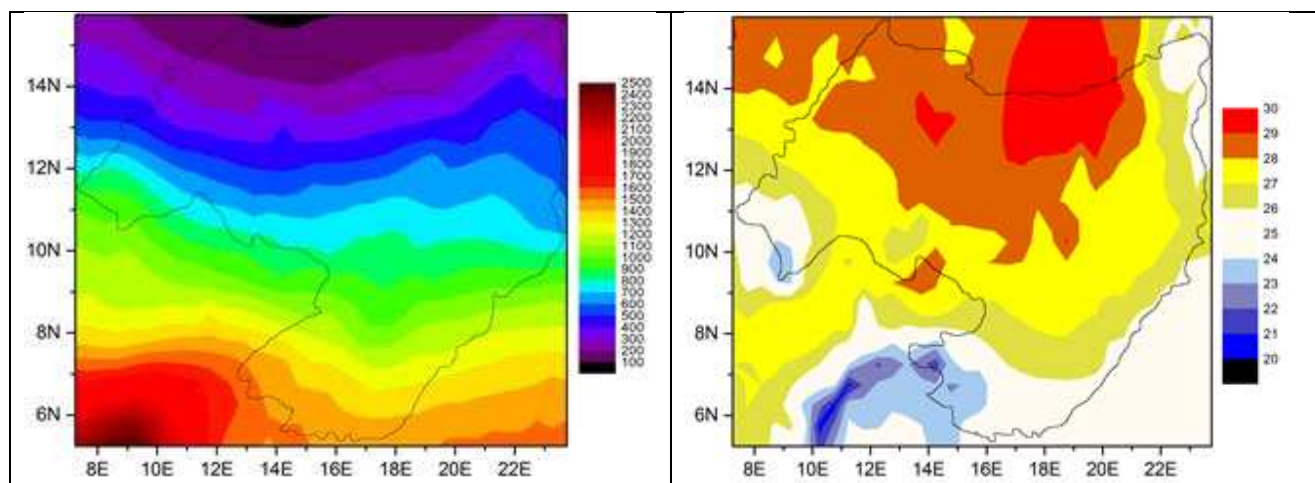
146 The Lake Chad basin (LCB) is located in Central Africa and lies between 5° - 24°N and 7° -
 147 24°E (Figure 2). The entire basin covers an estimated area of 2,434,000 km² shared by Algeria,
 148 Cameroon, Central Africa Republic, Chad, Libya, Niger, Nigeria and Sudan. This study focuses on
 149 the active drainage basin with an area of 1,053,455 km² (Adenle 2001) located between 5° - 16°N
 150 and 7° - 24°E (Cameroon, Central Africa Republic, Chad, Niger, Nigeria and Sudan). The reason
 151 for choosing only the active basin area is because, only this area contributes to inflows into the lake
 152 while the rest of the northern portion is covered by desert. Apart from some local mountains and
 153 plateaus located in northern and southern parts of the basin, the central part of the basin is very flat
 154 with an average slope of <1.3% (Le Coz et al. 2009; Nkiaka et al. 2017c).

155 Using data from Climate Research Unit (CRU) Time Series version 3.20 covering the period
 156 1901 – 2000, average rainfall over the basin was estimated to measure about 900 mm/year, varying
 157 between 1400 mm/year in the south to 370 mm/year in the north while average temperature was

158 estimated at 26.5°C. Figure 3 shows the contour plots of annual precipitation and average surface
159 temperature for the active basin area averaged over the period 1980 – 2005. The raining season in
160 the basin usually lasts from May to October with the highest rains recorded in August. The climate
161 in the basin is mostly hot and dry and rainfall is controlled by the north-south seasonal migration of
162 the intertropical convergence zone (ITCZ) as observed in the Logone catchment (Nkiaka et al.
163 2017b). 95% of inflows into the lake is contributed by the Logone and Chari rivers which originate
164 from the south (Odada et al. 2009).

165 Due to the high spatial variability in precipitation across the LCB, for the purpose of this
166 study, the active drainage basin was divided into three different ecological zones: 5° - 10°N
167 “Sudano”, 10° - 12°N “semi-arid” and 12° - 16°N “Arid”. These ecological zones represent some
168 simplified climatic zones based on Köeppen Geiger’s climate classification for Africa (Peel et al.
169 2007). Rainfall across all the ecological zones is unimodal with the peak occurring in August. The
170 highest rainfall is recorded in the Sudano zone while the lowest occurs in the arid zone. The CMIP5
171 models were assessed at the basin level and for each ecological zone. The advantage of this approach
172 is that in regions with high spatial variability and strong rainfall gradients such as the LCB, model
173 output averaged over the whole basin may lead to loss of signal such that the true expected change
174 could be larger than what is suggested by the model average (Knutti et al. 2010).

175
176



177 Figure 3: Contour plots for annual precipitation (left panel) and average surface
178 temperature (right panel) in the active basin area (1980 – 2005) calculated from CRU

179 3. Data

180 3.1. Observed Data

181 Due to the scarcity of observational data in the LCB, the observed rainfall and temperature
182 data used in this study was derived from climate research unit (CRU) Time Series version 3.20
183 dataset described by Harris et al. (2014) and made available free of charge by the British
184 Atmospheric Data Centre. This provides monthly-mean precipitation totals and average temperature
185 on a resolution of (0.5x0.5 degree) grids for the period 1901–2011. This dataset has been used as the
186 reference to evaluate CMIP5 models in previous studies e.g. (Rowell 2013; Miao et al. 2014;
187 Pattnayak et al. 2017). An additional precipitation dataset Watch Forcing Data methodology applied
188 to ERA-Interim (WFDEI) (Weedon et al. 2014) was used to complement the CRU dataset. WFDEI
189 has been applied for hydrological modelling studies in the Lake Chad basin (Nkiaka et al. 2017a)
190 and can be obtained from <https://dataguru.lu.se/>.

191

192 Table 1: List of climate models used in the study

Model No	Model Name	Institute/Country	Spatial Resolution Latitude X Longitude
M1	ACCESS1.0	Commonwealth Scientific Industrial and Research Organization, Bureau of Meteorology Australia	1.25 × 1.875
M2	BCC-CSM1.1-m	Beijing Climate Center, China	2.8 × 2.8
M3	CMCC-CMS	Centro Euro-Mediterraneo sui Cambiamenti Climatici Climate Model, Italy	2 x 2
M4	CNRM-CM5*	Centre National de Recherches Météorologiques, France	1.4 × 1.4
M5	GFDL-CM3	Geophysical Fluid Dynamics Laboratory, USA	
M6	HadGEM2-ES	Hadley Centre for Climate Prediction and Research, UK	1.875 × 1.25
M7	MPI-ESM-LR	Max Planck Institute for Meteorology, Germany	1.80 × 1.80

193

194 3.2. Climate model data

195 Climate model data used in this study was sourced from the 5th phase of the Coupled Model
196 InterComparison Project (CMIP5) (Taylor et al. 2012). The focus in this study is primarily on the
197 evaluation of the performance of these models in simulating the present-day (1980 – 2005) and
198 future climate projection by mid of the century (2050 – 2075) under two different RCPs (RCP4.5
199 and RCP8.5). The RCP4.5 is a stabilization scenario, in which the total radiative forcing is stabilized
200 before the end of the present century by the application of a range of technological innovations and
201 policies to reduce greenhouse gas (GHG) and aerosol emissions. On the other hand, the RCP8.5
202 scenario is considered a business as usual scenario characterized by increasing GHGs and aerosol
203 emissions leading to high concentrations beyond 2100. The labels for the RCPs provide a rough

204 estimate of the radiative forcing reaching the earth by the year 2100 (relative to preindustrial
205 conditions).

206 Although there are many models available from CMIP5 that can be used for impact studies,
207 not all models maybe able to simulate key climate processes across all regions of the globe. In this
208 study therefore, we selected CMIP5 models based on the fact that these models have been reported
209 in previous studies by Rowell (2013) and McSweeney et al. (2015) to “realistically” simulate some
210 key climate processes across Africa. These processes include: (i) annual cycles of precipitation and
211 temperature (ii) the West African monsoons and (iii) a minimum of 20 teleconnections in Africa.

212 Many other studies have also used a sub set of CMIP5 models (Brands et al. 2013; Schewe
213 et al. 2014; Pattnayak et al. 2017; Quesada et al. 2017). The models used in this study together with
214 their spatial resolution and country of origin are shown in Table 1. Monthly precipitation and average
215 temperature from each of the climate models and observed datasets was averaged over the whole
216 basin and for each ecological zone (Sudano, semi-arid and Arid). Analysis were conducted at annual
217 time scale for average temperature and annual and seasonal time scales for precipitation. The
218 seasonal precipitation was averaged for the months of June, July, August and September (monsoon
219 season). The reason for choosing this period was to evaluate the ability of the GCMs models to track
220 the movement of the “tropical rain belt” which some meteorologists suggest is responsible for
221 maximum rainfall in the region (Nicholson 2009; Nicholson 2013; Nicholson 2018) although this
222 assertion remains controversial among tropical meteorologists (Nicholson, 2018).

223 **4. Methodology**

224 The Reliability Ensemble Averaging (REA) technique (Giorgi and Mearns 2002) is based on
225 the assignment of weights to GCMs based on model evaluation. These weights are assigned on the
226 basis of model performance and model convergence. Details of the method are elaborated in the
227 following steps:

228 **Step1:** The simple model average method (SMA) whereby the estimated average change in
229 precipitation for all the models is calculated as:

230

$$231 \quad \overline{\Delta P} = \frac{1}{N} \sum_{i=1, N} \Delta P_i, \quad (1)$$

232

233 where N is the total number of models and the overbar indicates the ensemble averaging and ΔP
 234 indicates the model-simulated change in precipitation. In the SMA method, all models are given
 235 equal weight (One man, One-vote).

236 **Step 2:** The model reliability factor is calculated whereby, the average change, $\overline{\Delta P}$, is given by a
 237 weighted average of the ensemble members

238

$$239 \quad \overline{\Delta P} = \tilde{A}(\Delta P) = \frac{\sum_i^N R_i \Delta P_i}{\sum_i^N R_i}, \quad (2)$$

240

241 where the operator \tilde{A} denotes the REA averaging and R_i is the model reliability factor defined as

242

$$243 \quad R_i = [(R_{B,i})^m \times (R_{D,i})^n]^{[1/(m \times n)]} = \left\{ \left[\frac{\epsilon_p}{\text{abs}(B_{P,i})} \right]^m \left[\frac{\epsilon_p}{\text{abs}(D_{P,i})} \right]^n \right\}^{[1/(m \times n)]} \quad (3)$$

244

245 In Eq (3), R_i is the reliability factor, ϵ is the natural variability (as described in step 5 below). $R_{B,i}$
 246 is a factor that measures the model reliability as a function of the model bias ($B_{P,i}$) in simulating the
 247 present-day precipitation. It is defined as the difference between the model simulated estimate and
 248 observed and the higher the bias, the lower the model reliability. $R_{D,i}$ is a factor that measures the
 249 model reliability in terms of the distance ($D_{P,i}$) of the change calculated by a given model from the
 250 REA average change, the higher the distance, the lower the model reliability. Therefore, the distance
 251 is a measure of the degree of the model convergence of a given model with other ensemble members.
 252 In other words, $R_{B,i}$ is a measure of the model performance criterion while $R_{D,i}$ is a measure of the
 253 model convergence criterion.

254 **Step 3:** An iterative procedure is used to calculate the distance parameter $D_{P,i}$ starting with an initial
 255 guess value as the distance of each ΔP from the ensemble average change $\overline{\Delta P}$, as shown in Eq. (1),
 256 i.e. $[D_{P,i}]_1 = [\Delta P_i - \overline{\Delta P}]$. The first guess values are then substituted in Eq. (3) to obtain a first-order
 257 REA average change $[\overline{\Delta P}]_1$, which is then used to recalculate the distance of each individual model
 258 as $[D_{P,i}]_2 = [\Delta P_i - \overline{\Delta P}]_1$ and the iteration is repeated until the values converge. According to Giorgi
 259 and Mearns (2002), the distance from REA average is only an estimated measure of the model
 260 convergence criterion given that the future real conditions are not known.

261 **Step 4:** The parameter m and n in Eq. (3) can be used to weigh each criterion. In this study m and n
 262 are assumed to be 1, giving equal weight to both criteria. $R_{B,i}$ and $D_{P,i}$ are set to 1 when B and D are
 263 smaller than ϵ_P , respectively. Thus Eq. (3) states that the model projection is considered “reliable”
 264 when both its bias and distance from the ensemble average are within the natural variability ϵ , so
 265 that $R_B=D_P = 1$. As the bias and/or distance grow, the reliability of a given model simulation
 266 decreases.

267 **Step 5:** The parameter ϵ_P in Eq. (3) is a measure of natural variability in the 30-year average annual
 268 or seasonal precipitation and temperature. To calculate ϵ in this study, the time series of observed
 269 monthly precipitation and average temperature covering the period 1901 – 2005 obtained from CRU
 270 were employed. Then, 30-year moving averages of the series are calculated after linearly detrending
 271 the data (to remove century-scale trends), and ϵ estimated as the difference between the maximum
 272 and minimum values of these 30-year moving averages. Natural variability in rainfall and average
 273 temperature was calculated only for the whole basin.

274 **Step 6:** In order to calculate the uncertainty range around the REA average change, the REA root
 275 mean square difference (rmsd) of the changes $\tilde{\delta}_{\Delta P}$, has to be obtained and is defined by

$$277 \quad \tilde{\delta}_{\Delta P} = \left[\tilde{A}(\Delta P_i - \tilde{\Delta P})^2 \right]^{1/2} = \left[\frac{\sum_i R_i (\Delta P_i - \tilde{\Delta P})^2}{\sum_i R_i} \right]^{1/2} \quad (4)$$

278
 279 The upper and lower uncertainty limits are defined as

$$281 \quad \Delta P_+ = \tilde{\Delta P} + \tilde{\delta}_{\Delta P} \quad (5a)$$

$$282 \quad \Delta P_- = \tilde{\Delta P} - \tilde{\delta}_{\Delta P} \quad (5b)$$

283
 284 The total uncertainty range is then given by $\Delta P_+ - \Delta P_- = 2\tilde{\delta}_{\Delta P}$. According to the REA method, when
 285 the changes are distributed following a Gaussian PDF, the rmsd is equivalent to the standard
 286 deviation so that the $\mp\delta$ range would imply a 68.3% confidence interval. For a uniform PDF, that
 287 is, one in which each change has the same probability of occurrence, the $\mp\delta$ range implies a
 288 confidence interval of about 58%. Moreover, in the REA method, the normalized reliability factors
 289 of Eq. (3) are interpreted as the likelihood of a GCM outcome, meaning that; the greater the factor,

311 (160 – 240 mm). Furthermore, the MME monthly mean precipitation estimates were consistently
 312 lower than estimates from CRU and WFDEI across the basin and at the level of the ecological zones
 313 (Figure 4).

314 Agreement in observed and simulated monthly precipitation was also evaluated using Taylor
 315 diagram (Figure 5a). In the polar plot, the reference or observed data are plotted on the x-axis
 316 (abscissa), and the model-simulated values are expected to lie in the first quadrant if the correlation
 317 coefficient is positive. The radial dimension indicate the normalized standard deviation (calculated
 318 as the ratio of standard deviation of simulated over standard deviation of observed, ratios >1 indicate
 319 that the simulated values are more variable than observed), and the angular dimension shows the
 320 correlations. These statistics were computed using the 1980 – 2005 monthly precipitation. The
 321 similarity between model-simulated and observed precipitation is quantified in terms of their
 322 correlation and the amplitude of the variability. The correlation coefficients between each model and
 323 the monthly observations from CRU are in the range 0.50 – 0.95 and between the MME and
 324 observation is 0.85. This indicates that there are strong correlations between the estimates from the
 325 models and CRU. The strong correlation value between MME and CRU indicate that the MME
 326 performs slightly better than some individual GCM models (M1, M2, M3, M5, and M6). Models
 327 M4 and M7 show large variability compared to other models with normalized standard deviation >1
 328 although both models have high correlation coefficients >0.85.

329

330 Table 2: Model simulated biases of present-day precipitation (%) and average temperature (°C)

Time scale	Ecological Zone	GCM							
		M1	M2	M3	M4	M5	M6	M7	MME
Annual precipitation	LCB	12.11	13.39	-11.71	59.16	30.20	7.08	27.28	19.65
	Sudano	21.81	20.21	25.78	39.73	17.15	11.89	38.36	24.99
	Semi-arid	-6.07	-20.86	-33.70	82.14	17.31	-3.61	22.78	8.28
	Arid	-51.86	-59.17	-82.19	48.37	27.35	-38.63	2.80	-21.90
Monsoon (JJAS) precipitation	LCB	-26.08	-41.14	-32.77	35.51	-12.65	-22.88	9.24	-12.97
	Sudano	-8.16	-20.93	-3.93	20.55	-9.30	-11.10	13.61	-2.75
	Semi-arid	-28.31	-48.72	-40.38	57.59	-18.31	-23.04	12.41	-12.68
	Arid	-62.74	-73.90	-84.99	31.77	-10.58	-49.22	-6.02	-36.52
Annual average temperature	LCB	-2.98	-2.31	-2.96	-6.03	-4.37	-4.69	-3.85	-3.88
	Sudano	-2.30	-2.17	-3.27	-4.99	-4.68	-3.75	-4.22	-3.62
	Semi-arid	-2.80	-2.33	-2.35	-6.79	-4.28	-4.80	-4.25	-3.94
	Arid	-3.83	-2.42	-3.25	-6.33	-4.16	-5.52	-3.09	-4.09

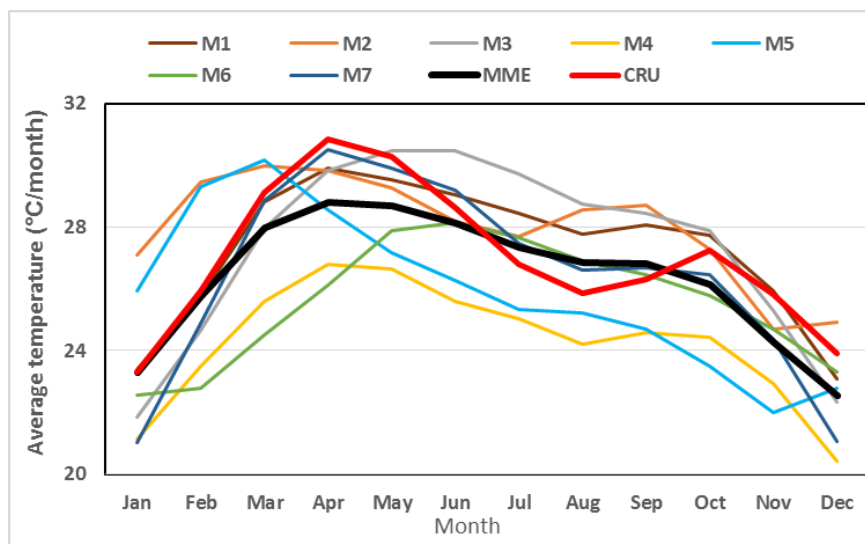
331

332 As a first step to quantify uncertainty using the REA method, the model performance criteria
 333 based on its ability to simulate the present-day climate was assessed using the bias factor. At the

356 temperature was in the range 0.40 – 0.90. However, most GCMs show large variability with
 357 normalized standard deviations >1 (M1, M3, M5, M6, M7). Four models produced correlation
 358 coefficients >0.75 which could be considered as strong. Meanwhile, the MME produced a
 359 correlation coefficient of 0.86 stronger than what was obtained for some individual models (M2,
 360 M5, and M6).

361 The model performance criteria based on its ability to simulate the present-day climate was
 362 also assessed using the bias factor. At the annual time-scale all the GCMs produced negative biases,
 363 underestimating present-day average temperature throughout the LCB and at the level of the
 364 different ecological zones indicating a generalized cold bias. Average temperature was
 365 underestimated in the range of (-2°C) – (-6°C) (Table 2). These results are contrasting with those of
 366 precipitation whereby varied results showing both positive and negative biases were obtained.

367



368

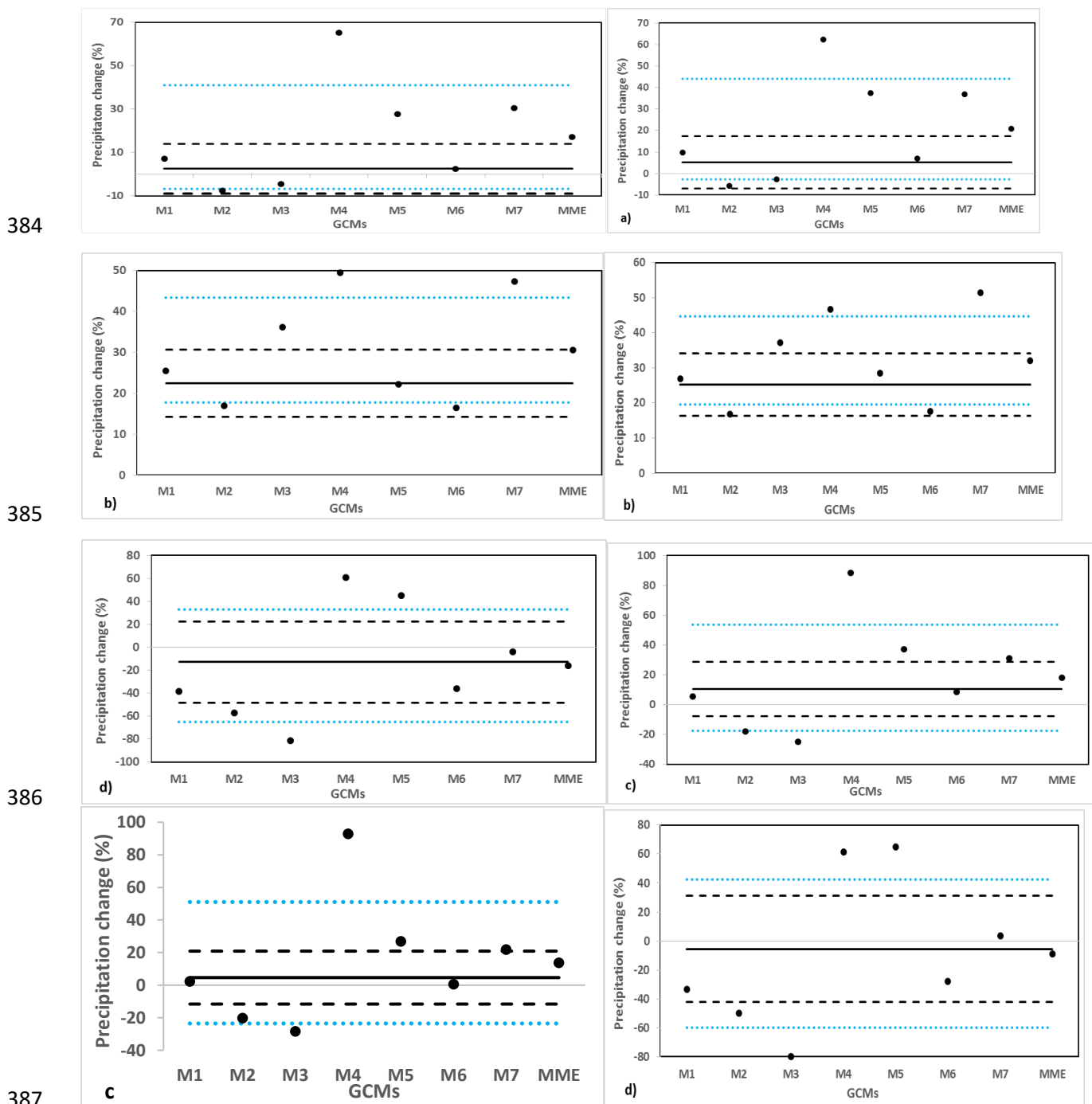
369

Figure 6: Annual temperature cycle over the Lake Chad basin

370 5.3. Future annual precipitation projections in the LCB (2050 – 2075)

371 Analysis using the REA technique indicate that, future annual precipitation in the LCB is
 372 projected to increase by about 2.5% across the basin under the RCP4.5 scenario relative to the
 373 historical period (1980 – 2005). At the level of the different ecological zones, future annual
 374 precipitation is projected to increase by 22% in the Sudano zone, 4% in the semi-arid and a decline
 375 of about -12% in the arid zone relative to the historical period. Under the RCP8.5 scenario, future
 376 annual precipitation is projected to increase by about 5% across the LCB which is double the RCP4.5
 377 scenario. These results corroborate the findings of Aloysius et al. (2016) in the Central Africa region

378 covering the LCB whereby, the authors also projected an increase in precipitation in the region from
 379 an ensemble of CMIP5 models by the end of the present century. At the level of ecological zones,
 380 projections for future annual precipitation is projected to increase by 30%, 9% and 5% for the
 381 Sudano, semi-arid and arid zones respectively. Under the RCP8.5 scenario, the Sudano zone show
 382 an increase of about 8% higher than the projection from RCP4.5 scenario while the arid zone may
 383 experience a drop of about of about -5% relative to the historical period (Table 3 and Figure 7).



388

389

390

391

392

393

394

395

396

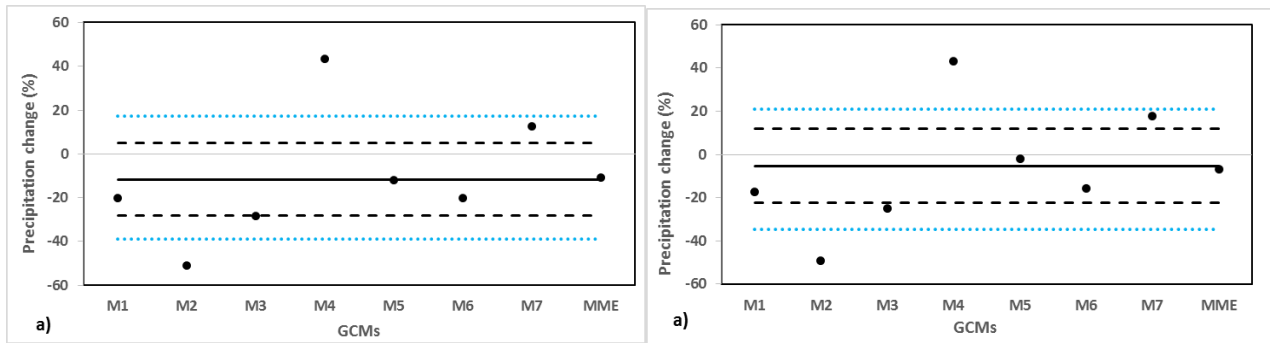
397



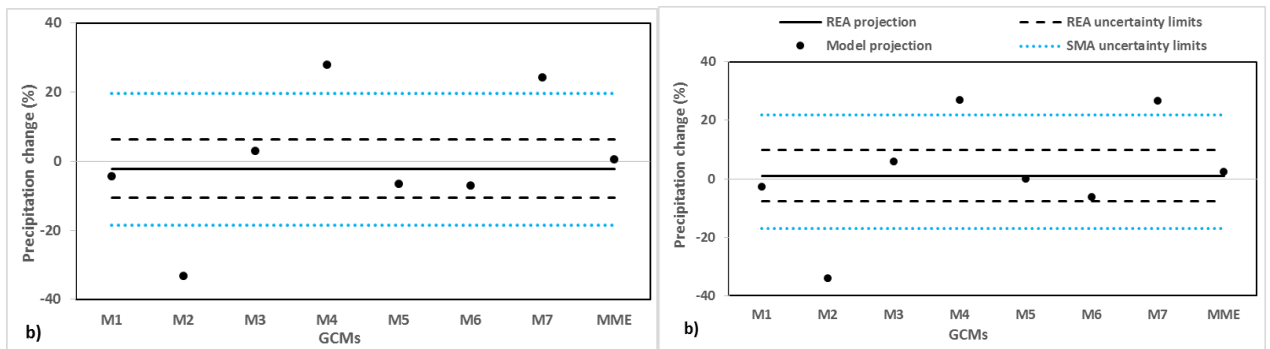
Figure 7: Annual precipitation projection under RCP4.5 (first column) and RCP8.5 (second column) a – d represents the LCB, sudano, semi-arid and arid zones respectively

Monsoon precipitation is projected to decrease across the basin by -11% and 5% under the RCP4.5 and RCP8.5 respectively. At the level of the different ecological zones monsoon precipitation is also projected to decrease across all the ecological zones and for both scenarios under investigation (Table 3 and Figure 8).

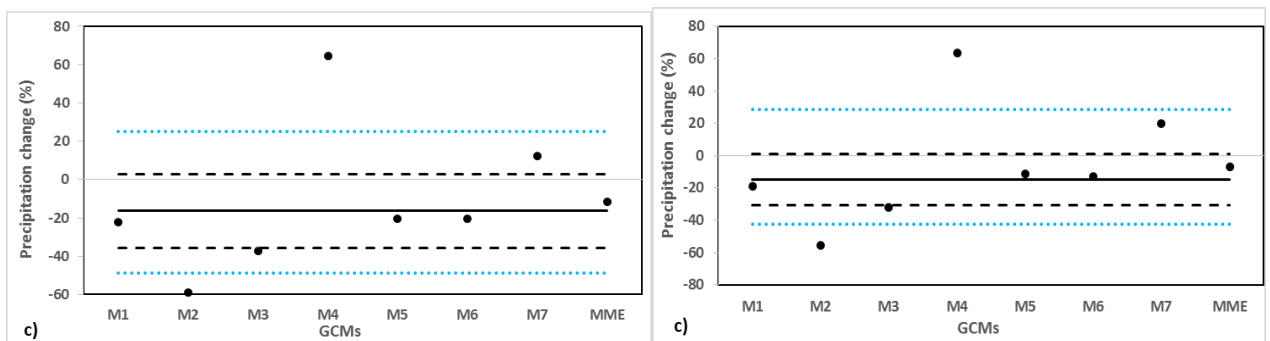
398

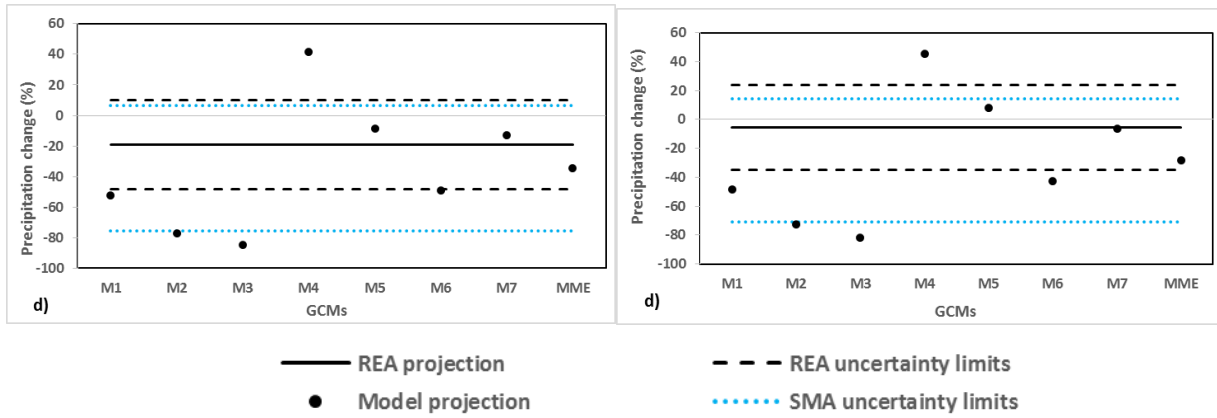


399



400





401

402

403

404

405

406

407

408

409

410

411

412

413

414

415

416

417

418

419

420

421

422

423

424

425

426

Figure 8: Seasonal precipitation projection under RCP4.5 (first column) and RCP8.5 (second column), a – d represents the LCB, sudano, semi-arid and arid zones respectively

Regarding the uncertainties in future precipitation projections, the REA average changes are all within the range of natural variability ϵ_P across the LCB under the two concentration pathways RCP4.5 and RCP8.5 (Table 3). Although this does not discount the fact that the changes in future precipitation are not statistically significant. At the level of the different ecological zones, the uncertainty range is also in the same order of magnitude with the natural variability although there is an increase of more than 10% in the arid zone. Comparing the three different ecological zones together, uncertainty is lower in the Sudano zone while the arid zone displays the highest level of uncertainty which follows the same trend that was observed for natural variability (Table 3).

Considering projections from individual CMIP5 models, under the RCP4.5 scenario, M1, M4, M5, M6, and M7 project an increase in future annual precipitation while M2, and M3 project a decrease at the basin scale. M1 M2, M3 and M6 lie within the uncertainty range but only M1 and M6 project and increase while M2 and M3 project a decrease (Figure 7a). The results are varied for the different ecological zones. In the Sudano zone, all models project an increase in future annual precipitation with M1, M2, M5, and M6 lying within the uncertainty range (Figure 7b). Within the semi-arid zone, all models project an increase in future precipitation except M2 and M3, although only projections from M1, M6 and M7 fall within the uncertainty range (Figure 7c). In the arid zone only M4 and M5 project an increase in future precipitation although their results are outside the uncertainty range while the rest project a decrease. (Figure 7d).

Under the RCP4.5 scenario, M4 and M7 project an increase in future monsoon precipitation while the other models project a decrease at basin scale with results lying outside the uncertainty range (not shown). In the Sudano zone, M3, M4 and M7 project an increase in future monsoon

427 precipitation while the other models project a decrease although only projections from M3 lie within
 428 the uncertainty range (not shown). Results in the semi-arid zone are similar to those obtained in the
 429 Sudano zone. In the arid zone, only M4 project an increase in future monsoon precipitation while
 430 the rest of models project a decrease however and results do not lie within the uncertainty range (not
 431 shown).

432 Under the RCP8.5 scenario, future annual precipitation is projected to increase across the
 433 LCB by all models except M2 and M3 with projections from M1 and M6 lying within the uncertainty
 434 range (Figure 7a). In the Sudano zone, all models project an increase in future annual precipitation
 435 with projections from M1, M2, M5 and M6 lying within the uncertainty range (Figure 8b). In the
 436 semi-arid zone, all models except M2 and M3 project an increase with projections from M1 and M6
 437 lying within the uncertainty range (Figure 7c). Model M4, M5 and M7 project an increase in the arid
 438 zone while the other models project a decrease with projections from M7 lying within the uncertainty
 439 range. Individual model projections for monsoon precipitation under this scenario are similar to what
 440 was obtained under the RCP4.5 scenario although with different magnitudes (not shown).

441

442 Table 3: Natural variability, projected precipitation change and uncertainty range

Time scale	Ecological zone	Natural variability (ϵP) (mm)	RCP4.5		RCP8.5	
			ΔP (%)	Uncertainty ($\pm\delta\Delta P$)	ΔP (%)	Uncertainty ($\pm\delta\Delta P$)
Annual precipitation	LCB	84.40 (11.43)	2.54	11.37	5.26	12.13
	Sudano	81.81 (7.24)	22.61	8.29	30.56	8.97
	Semi-arid	95.23 (11.89)	4.15	15.69	9.72	16.92
	Arid	88.33 (23.15)	-12.32	34.77	-4.77	36.34
Monsoon precipitation	LCB	16.45 (11.32)	-11.61	16.52	-5.29	17.11
	Sudano	12.68 (6.38)	-0.72	12.55	3.14	12.39
	Semi-arid	21.59 (14.44)	-16.63	18.39	-9.28	18.58
	Arid	20.75 (23.59)	-23.11	25.49	-13.79	28.35

443 *The values in bracket represent the percentage change in precipitation relative to the historical period (1980 – 2005)

444 **5.4. Future average temperature projections in the LCB (2050 – 2075)**

445 Analysis using the REA technique show that future annual average temperature across the
 446 LCB under the RCP4.5 and RCP8.5 scenarios is projected to decrease by about 1°C relative to the
 447 historical period (1980-2005) and by almost the same amount across the different ecological zones
 448 (Table 4). These results are quite contrasting to what has been observed globally from CMIP5
 449 models which generally project an increase in future global average temperatures (Knutti and
 450 Sedláček 2013) and in the African continent (Dike et al. 2015).

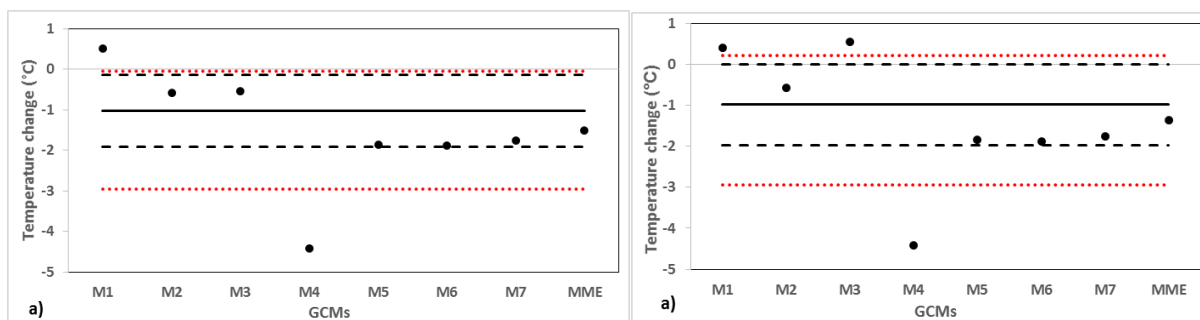
451 Regarding uncertainty in the future annual average temperature projections, the REA average
 452 changes are outside the range of natural variability ϵ_T across the LCB and at the level of the different
 453 ecological zones under both RCPs. Natural variability in annual average temperature is highest in
 454 the arid zone and lowest in the Sudano zone. However, uncertainty in model projections of annual
 455 average temperature is highest in the semi-arid zone and lowest in the arid zone (Figure 9).

456 Considering future projections from individual CMIP5 models, under the RCP4.5 scenario,
 457 only M1 consistently projects an increase in future annual average temperature over the LCB and at
 458 the level of different ecological zones while all the other models project a decrease (Figure 8). Under
 459 the RCP8.5 scenario, M1 and M3 consistently project an increase in projected future annual
 460 temperature over the basin and at the level of the Sudano and semi-arid zones while only M3 project
 461 an increase in the arid zone. The projections from models showing an increase in future average
 462 temperature all lie outside the uncertainty range while the results are mixed for those projecting a
 463 decrease (Figure 9).

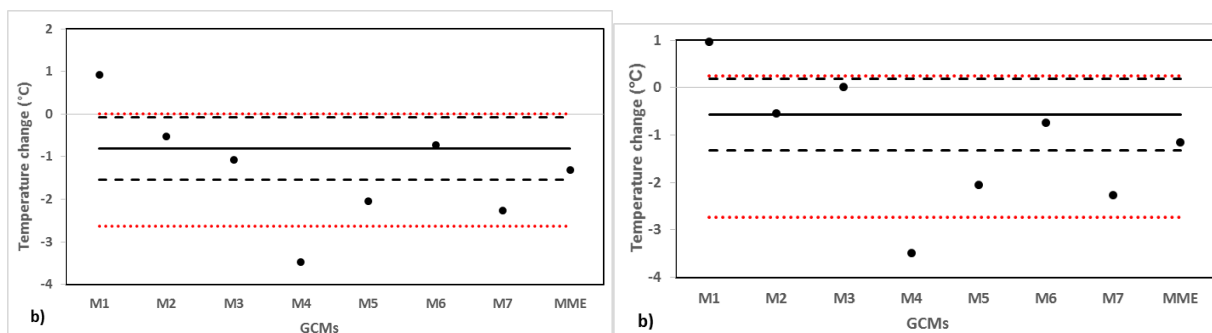
464 Table 4: Natural variability, projected temperature change and uncertainty range

Time scale	Ecological zone	Natural variability (ϵ_T) (°C)	RCP4.5		RCP8.5	
			ΔT (°C)	Uncertainty ($\pm\delta\Delta T$)	ΔT (°C)	Uncertainty ($\pm\delta\Delta T$)
Annual average temperature	LCB	0.50	-1.02	0.89	-0.99	0.98
	Sudano	0.28	-0.84	0.78	-0.55	0.90
	Semi-arid	0.48	-0.70	1.04	-0.70	1.19
	Arid	0.68	-0.85	0.72	-0.72	0.79

465

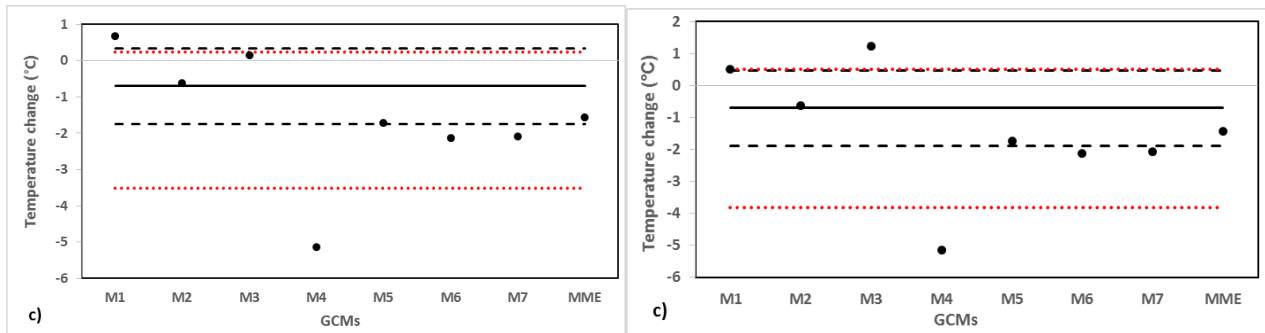


466

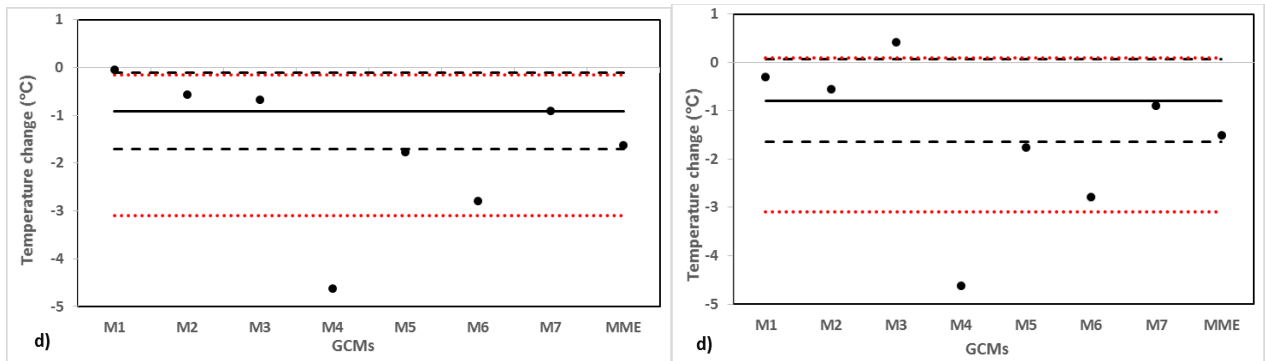


467

468



469



470



471 Figure 9: Annual average temperature projection under RCP4.5 (first column) and RCP8.5 (second
 472 column) a – d represents the LCB, sudano, semi-arid and arid zones respectively

473

474 5.5. Reliability analysis of CMIP5 models for precipitation and temperature 475 projections

476 Under RCP4.5 and RCP8.5, M1, M2, M3 and M6 produced model reliability factors ≥ 0.85
 477 for future annual precipitation projection in the LCB and all projections from these models lie within
 478 the REA uncertainty range (Figure 7a). This performance can be attributed to the fact that, (i) the
 479 bias factor (difference between the model simulated estimate and observed), and under both RCPs
 480 (ii) the convergence factor (distance between the model projection and REA average) for each of the
 481 models are within the bounds of natural variability ϵ_p . Models with low reliability factors equally
 482 produced low bias and convergence factors (Table 5) and projections from these models all lie
 483 outside the REA uncertainty range (Figure 7a).

484 At the seasonal scale only M5 produced a reliability factor > 0.80 and the projection from this
 485 model is very close to the REA average. The low performance of the CMIP5 models for monsoon
 486 projection can be attributed to the fact that apart from M5 and M7, most of the models produced
 487 very low bias factors mostly below 0.5 as a result of their consistent underestimation of monsoon

488 precipitation relative to the historical period. It can also be observed that even though M1, M3, and
489 M6 produced very high convergence factors for projected monsoon precipitation, these models were
490 penalized because of their low bias factors. On the other hand, M7 which produced a high bias factor
491 for monsoon precipitation was penalized because of its low convergence factor (Table 5). By given
492 equal weights to criteria m and n in Eq. (3) any model which performs well in one criteria and does
493 not equally perform well in the other is penalized.

494 The reliability factors of the various models for annual average temperature projection in the
495 LCB under RCP4.5 and RCP8.5 scenarios are generally very low with some values <0.10 . This low
496 performance can be attributed to the inability of the models to simulate historical annual average
497 temperature resulting in a generalized low bias factors among the CMIP5 models. Even though all
498 models except M1 and M4 under the RCP4.5 scenario and M2, M5, M6 and M7 under the RCP8.5
499 scenario produced high convergence factors, these models were penalized because of their low
500 ability to simulate historical average temperature.

501 Comparing the results from REA average and simple model average (SMA) or MME for
502 annual and seasonal precipitation projections, it was observed that, under the two RCPs, estimates
503 from SMA (MME) do not deviate significantly from the REA average and in most cases lie within
504 the REA uncertainty range (Figures 7 - 8). This shows that both methods produce ensemble averages
505 that are similar in magnitude. This is an interesting finding given that each model received a different
506 weight through the application of either techniques. In the SMA (MME) technique, each model
507 received the same weight while with REA technique the weight attached to each model was based
508 on its reliability factor which was determined by both the bias and convergence factors. Previous
509 studies have also shown that both methods produced similar results e.g. (Miao et al. 2014; Mani and
510 Tsai 2016). However, it can also be observed from the figures that the uncertainty range for SMA is
511 larger than that of REA technique

512
513
514
515
516
517
518

519

520 Table 5 Model performance for historical and future projections for annual and monsoon precipitation

Model	Annual precipitation					Monsoon precipitation				
	Bias factor	RCP 45		RCP 85		Bias factor	RCP 45		RCP 85	
		Convergence factor	Reliability factor	Convergence factor	Reliability factor		Convergence factor	Reliability factor	Convergence factor	Reliability factor
M1-ACCESS1.0	0.94	1.00	0.94	1.00	0.94	0.43	1.00	0.43	0.96	0.42
M2-bcc_ESM1-1-M	0.85	1.00	0.85	1.00	0.85	0.28	0.29	0.08	0.26	0.07
M3-CMCC_CMS	0.98	1.00	0.98	1.00	0.98	0.35	0.66	0.23	0.59	0.20
M4-CNRM-CM5	0.19	0.18	0.04	0.20	0.04	0.32	0.21	0.07	0.23	0.07
M5-GFDL-CM	0.38	0.46	0.17	0.36	0.13	0.89	1.00	0.89	1.00	0.89
M6-HadGEM-ES	1.00	1.00	1.00	1.00	1.00	0.49	1.00	0.49	1.00	0.49
M7-MPI-ESM-LR	0.42	0.41	0.17	0.36	0.15	1.00	0.47	0.47	0.48	0.48

521 *Note that the different ecological zones are not considered

522

524 **6. Discussion**

525 Given the fact that some models showed systematic biases in the seasonal rainfall estimates
526 indicate that they were not able to track the north-south displacement of the ITCZ as they are
527 consistently too wet in the dry season, and too dry in the wet season.

528 The fact that MME (SMA) produced stronger correlations compared to some individual
529 models in the Taylor diagram for both precipitation and average temperature can be attributed to the
530 fact that, by averaging all the models together, the individual model biases cancel out thus resulting
531 to an ensemble that outperforms some of the individual CMIP5 models.

532 Even though the CMIP5 models used in this study were reported to simulate some key
533 climate processes in the region based on the findings of Rowell (2013) and McSweeney et al. (2015),
534 results from our study show that, there was still a large spread in the model output which can be
535 attributed to individual model physics. Despite this spread, most of the models were able to replicate
536 the historical annual rainfall cycle across the basin and at the level of the different ecological zones
537 indicating some level of objectivity in the selection process. Furthermore, the ensemble projections
538 from the MME (SMA) average were mostly within the bounds of uncertainty limits across the basin
539 and at the level of the ecological zone which can also be attributed to the model selection process.

540 Apart from biases associated with model physics, biases in the model simulations could also
541 be attributed to the inability of the individual CMIP5 model to simulate other local scale atmospheric
542 processes and mesoscale convective systems (MCSs) and non-climatic effects like orography that
543 also influence climate in the region (Nkiaka et al., 2017c). This is largely due to their coarse spatial
544 resolutions. In fact, MCSs are difficult to be modelled because these events organize dynamically
545 on spatial scales that cannot be resolved by the current generation of GCMs (Taylor et al. 2017).
546 Other mechanisms that influence regional climate in LCB include the low level Bodele Jets
547 (Washington et al. 2006), the high level Tropical Easterly Jets (TEJ) and the West African Westerly
548 Jets (WAWJ) which are stronger in the eastern Sahel where the LCB is located (Nicholson 2013)
549 and the high level African Easterly Jet (AEJ) which influence precipitation over the Central African
550 region (Farnsworth et al. 2011). It is not known how these jet streams are simulated in the CMIP5
551 models although their influence on regional rainfall is very significant (Nicholson et al., 2013).

552 Despite the poor performance of the GCMs to continuously underestimate historical
553 monsoon precipitation in this study, previous studies also reported the decline in monsoon

554 precipitation in the region (Polson et al. 2014; Nkiaka et al. 2017b) albeit causes of this decline are
555 not yet well understood. Nevertheless, Devaraju et al. (2015) attributed it to large scale deforestation
556 in the northern middle and high latitudes which force the ITCZ to shift southwards resulting in a
557 significant decrease in monsoon precipitation. Quesada et al. (2017) also attributed the decline in
558 monsoon precipitation in historical and future climate projections to biophysical effects of large
559 scale land use/cover changes. Despite this, recent studies by Taylor et al. (2017) have shown that,
560 extreme precipitation events from MCSs during the monsoon season has increased in the region.
561 Nonetheless the study by Taylor et al. (2017) did not mention the contribution of MCSs extreme
562 precipitation events to the total monsoon precipitation although their contribution to total annual
563 precipitation in that study was estimated to be < 25%.

564 Generally, results from this study show an increase in projected annual precipitation by mid
565 of the century with five models projecting this increase under both RCPs. These results are also
566 supported by the MME (SMA) average whereby equal weights are attached to each model and REA
567 average whereby weights are attached to a model based on the model reliability factor. In each case,
568 future annual precipitation is projected to increase in the LCB. At the level of the different ecological
569 zones, all models project an increase in future precipitation in the Sudano, five models project an
570 increase in the semi-arid and three models project an increase in the arid zone under both RCPs.

571 Another significant finding from this study is the fact that, although CMIP5 models project
572 a decrease in future monsoon precipitation which is known to contribute to most of the rainfall in
573 the region, overall, annual precipitation is still projected to increase by the middle of the century
574 under both RCPs. This implies that in future, the seasonal north – south migration of the ITCZ which
575 brings monsoon precipitation into the region may no longer be the dominant mechanism responsible
576 for rainfall in the region. This is consistent with other studies in the region that have reported of a
577 dryer onset of the monsoon season and an intensification of the late rainy season (Biasutti 2013).
578 Another study by Monerie et al. (2016) has also reported of an increase in late rainy season
579 (September and October) rainfall and a delay in the retreat of the monsoon. This can partly explain
580 why even though the CMIP5 models are projecting a decrease in monsoon precipitation, annual
581 precipitation is still projected to increase across the LCB.

582 The increase in projected annual precipitation in the region under climate change have been
583 attributed to many reasons e.g. Dong and Sutton (2015) attribute it to the rising levels of GHGs in
584 the atmosphere, Evan et al. (2015) attribute it to an upward trend in the Sahara heat low (SHL)
585 temperature resulting from atmospheric greenhouse warming by water vapor. In separate studies,

586 Biasutti (2013) and Park et al. (2015) attributed the increase in future precipitation in the region as
587 projected by CMIP5 models to increased moisture convergence in the region under climate change.
588 Generally, the models were biased in simulating historical and future projected average temperature
589 in the LCB. The poor performance by GCMs in simulating average surface temperature in this study
590 may be attributed to increased insolation over region considering that the region is known to be one
591 of the cloudiest in the tropics; it could also be attributed to large biases in GCMs in simulating cloud
592 climatology (Lauer and Hamilton 2013; Diallo et al. 2014; Dommo et al. 2018).

593 **7. Conclusion**

594 The objectives of this study were to evaluate the ability of CMIP5 models to reproduce the
595 present-day climate conditions in the LCB (1980-2005), assess the future climate projections for the
596 basin by the middle of century (2050 – 2075) relative to the historical period and quantify the
597 uncertainties associated with these projections using two Representative Concentration Pathways
598 (RCP4.5 and 8.5). This is the first study that uses climate models to assess future precipitation and
599 average temperature projections in the LCB. Results indicate an increase in precipitation across the
600 study domain under RCP4.5 and RCP8.5 by mid of the century, with the Sudano zone expected to
601 experience the highest amount of future annual precipitation.

602 Results further indicate that, the CMIP5 models simulated precipitation better than
603 temperature as a result of a cold bias observed in the simulation of annual average temperature by
604 the models. Although results from the study vary from one model to another, overall M4 performed
605 poorly as it consistently overestimated future projected precipitation and underestimated annual
606 average temperature across the basin and at the level of the different ecological zones under both
607 RCPs. In addition, no projections from this model lie within the uncertainty range suggesting that,
608 M4 is an outlier within the ensemble used in this study and may not be recommended for future
609 impact studies in the LCB. For impact studies in the LCB using CMIP5 models, M1 and M6 with
610 future precipitation projections that consistently lie within the REA uncertainty limits under both
611 RCPs may be recommended. Meanwhile M1 which projected increasing temperature trends in
612 agreement with global and continental trends may be recommended for impact studies in the basin.
613 Overall M1 will be suitable for hydrological modelling studies in the LCB.

614 Results from this study also show that the REA technique which uses a reliability factor
615 whereby weights are attached to a model based on its ability to simulate both the present-day climate
616 through the bias factor and future climate through the convergence factor is a robust method to

617 considerably reduce uncertainties in climate models to compared to the Simple model averaging
618 (SMA) technique. The weights attached to each model is calculated based on past natural climate
619 variability observed in the area. Using this approach, uncertainty limits obtained in this study
620 especially for precipitation were mostly within the bounds of natural rainfall variability across the
621 LCB.

622 Nevertheless, biases observed in the models could be reduced and results obtained in this
623 study refined by using regional climate models. Results could also be fine – tuned in future as high
624 resolution GCMs become available.

625

626 **Acknowledgements**

627 The first author is sponsored by the Commonwealth Scholarship Commission in the UK. The authors
628 are grateful to CRU for making their datasets available for this study. Thanks are also due to IPCC
629 for providing the CMIP5 data freely for research purpose. We are also indebted to Dr. Rory
630 Fitzpatrick, School of Earth and Environment, University of Leeds for helping us download CMIP5
631 model output.

632

633 **References**

- 634 ADENLE, D. 2001. *Groundwater resources and environmental management in Niger Basin Authority and Lake*
635 *Chad Basin Commission agreements*. UIPO, Ibadan, Nigeria.
- 636 AKURUT, M., P. WILLEMS and C. NIWAGABA. 2014. Potential Impacts of Climate Change on Precipitation
637 over Lake Victoria, East Africa, in the 21st Century. *Water*, **6**(9), p2634.
- 638 ALOYSIUS, N. R., J. SHEFFIELD, J. E. SAIERS, H. LI and E. F. WOOD. 2016. Evaluation of historical and future
639 simulations of precipitation and temperature in central Africa from CMIP5 climate models. *Journal*
640 *of Geophysical Research: Atmospheres*, **121**(1), pp.130-152.
- 641 ARMITAGE, S. J., C. S. BRISTOW and N. A. DRAKE. 2015. West African monsoon dynamics inferred from
642 abrupt fluctuations of Lake Mega-Chad. *Proceedings of the National Academy of Sciences*, **112**(28),
643 pp.8543-8548.
- 644 ARNELL, N. W. 2004. Climate change and global water resources: SRES emissions and socio-economic
645 scenarios. *Global environmental change*, **14**(1), pp.31-52.
- 646 BIASUTTI, M. 2013. Forced Sahel rainfall trends in the CMIP5 archive. *Journal of Geophysical Research:*
647 *Atmospheres*, **118**(4), pp.1613-1623.
- 648 BRANDS, S., S. HERRERA, J. FERNÁNDEZ and J. M. GUTIÉRREZ. 2013. How well do CMIP5 Earth System
649 Models simulate present climate conditions in Europe and Africa? *Climate dynamics*, **41**(3-4),
650 pp.803-817.
- 651 DEVARAJU, N., G. BALA and A. MODAK. 2015. Effects of large-scale deforestation on precipitation in the
652 monsoon regions: Remote versus local effects. *Proceedings of the National Academy of Sciences*,
653 **112**(11), pp.3257-3262.

654 DIALLO, I., C. L. BAIN, A. T. GAYE, W. MOUFOUMA-OKIA, C. NIANG, M. D. DIENG and R. GRAHAM. 2014.
655 Simulation of the West African monsoon onset using the HadGEM3-RA regional climate model.
656 *Climate dynamics*, **43**(3-4), pp.575-594.

657 DIKE, V. N., M. H. SHIMIZU, M. DIALLO, Z. LIN, O. K. NWOFOR and T. C. CHINEKE. 2015. Modelling present
658 and future African climate using CMIP5 scenarios in HadGEM2-ES. *International Journal of*
659 *Climatology*, **35**(8), pp.1784-1799.

660 DOMMO, A., N. PHILIPPON, D. A. VONDOU, G. SÈZE and R. EASTMAN. 2018. The June-September low cloud
661 cover in Western Central Africa: mean spatial distribution and diurnal evolution, and associated
662 atmospheric dynamics. *Journal of Climate*, (2018).

663 DONG, B. and R. SUTTON. 2015. Dominant role of greenhouse-gas forcing in the recovery of Sahel rainfall.
664 *Nature Climate Change*, **5**(8), pp.757-760.

665 EVAN, A. T., C. FLAMANT, C. LAVAYASSE, C. KOCHA and A. SACI. 2015. Water vapor–forced greenhouse
666 warming over the Sahara Desert and the recent recovery from the Sahelian drought. *Journal of*
667 *Climate*, **28**(1), pp.108-123.

668 FARNSWORTH, A., E. WHITE, C. J. R. WILLIAMS, E. BLACK and D. R. KNIVETON. 2011. Understanding the
669 Large Scale Driving Mechanisms of Rainfall Variability over Central Africa. In: C. J. R. WILLIAMS and
670 D. R. KNIVETON, eds. *African Climate and Climate Change: Physical, Social and Political Perspectives*.
671 Dordrecht: Springer Netherlands, pp.101-122.

672 FOTSO-NGUEMO, T. C., D. A. VONDOU, C. TCHAWOUA and A. HAENSLER. 2017. Assessment of simulated
673 rainfall and temperature from the regional climate model REMO and future changes over Central
674 Africa. *Climate dynamics*, **48**(11-12), pp.3685-3705.

675 GIORGI, F. and L. O. MEARNS. 2002. Calculation of average, uncertainty range, and reliability of regional
676 climate changes from AOGCM simulations via the “reliability ensemble averaging”(REA) method.
677 *Journal of Climate*, **15**(10), pp.1141-1158.

678 GOSLING, S. N. and N. W. ARNELL. 2016. A global assessment of the impact of climate change on water
679 scarcity. *Climatic Change*, **134**(3), pp.371-385.

680 HAENSLER, A., F. SAEED and D. JACOB. 2013. Assessing the robustness of projected precipitation changes
681 over central Africa on the basis of a multitude of global and regional climate projections. *Climatic*
682 *Change*, **121**(2), pp.349-363.

683 HARRIS, I., P. JONES, T. OSBORN and D. LISTER. 2014. Updated high-resolution grids of monthly climatic
684 observations—the CRU TS3. 10 Dataset. *International Journal of Climatology*, **34**(3), pp.623-642.

685 KATZ, R. W., P. F. CRAIGMILE, P. GUTTORP, M. HARAN, B. SANSÓ and M. L. STEIN. 2013. Uncertainty analysis
686 in climate change assessments. *Nature Climate Change*, **3**(9), pp.769-771.

687 KNUTTI, R., R. FURRER, C. TEBALDI, J. CERMAK and G. A. MEEHL. 2010. Challenges in combining projections
688 from multiple climate models. *Journal of Climate*, **23**(10), pp.2739-2758.

689 KNUTTI, R. and J. SEDLÁČEK. 2013. Robustness and uncertainties in the new CMIP5 climate model
690 projections. *Nature Climate Change*, **3**(4), pp.369-373.

691 KOUTSOYIANNIS, D., A. EFSTRATIADIS and K. P. GEORGAKAKOS. 2007. Uncertainty Assessment of Future
692 Hydroclimatic Predictions: A Comparison of Probabilistic and Scenario-Based Approaches. *Journal*
693 *of Hydrometeorology*, **8**(3), pp.261-281.

694 LAUER, A. and K. HAMILTON. 2013. Simulating clouds with global climate models: A comparison of CMIP5
695 results with CMIP3 and satellite data. *Journal of Climate*, **26**(11), pp.3823-3845.

696 LE COZ, M., F. DELCLAUX, P. GENTHON and G. FAVREAU. 2009. Assessment of Digital Elevation Model (DEM)
697 aggregation methods for hydrological modeling: Lake Chad basin, Africa. *Computers & Geosciences*,
698 **35**(8), pp.1661-1670.

699 MANI, A. and F. T.-C. TSAI. 2016. Ensemble Averaging Methods for Quantifying Uncertainty Sources in
700 Modeling Climate Change Impact on Runoff Projection. *Journal of Hydrologic Engineering*,
701 p04016067.

702 MCSWEENEY, C., R. JONES, R. LEE and D. ROWELL. 2015. Selecting CMIP5 GCMs for downscaling over
703 multiple regions. *Climate dynamics*, **44**(11-12), pp.3237-3260.

704 MEEHL, G. A., T. F. STOCKER, W. D. COLLINS, A. FRIEDLINGSTEIN, A. T. GAYE, J. M. GREGORY, A. KITOH, R.
705 KNUITTI, J. M. MURPHY and A. NODA. 2007. Global climate projections.

706 MEHRAN, A., A. AGHAKOUCHAK and T. J. PHILLIPS. 2014. Evaluation of CMIP5 continental precipitation
707 simulations relative to satellite-based gauge-adjusted observations. *Journal of Geophysical*
708 *Research: Atmospheres*, **119**(4), pp.1695-1707.

709 MIAO, C., Q. DUAN, Q. SUN, Y. HUANG, D. KONG, T. YANG, A. YE, Z. DI and W. GONG. 2014. Assessment of
710 CMIP5 climate models and projected temperature changes over Northern Eurasia. *Environmental*
711 *Research Letters*, **9**(5), p055007.

712 MIN, S.-K. and A. HENSE. 2006. A Bayesian approach to climate model evaluation and multi-model averaging
713 with an application to global mean surface temperatures from IPCC AR4 coupled climate models.
714 *Geophysical Research Letters*, **33**(8), pp.n/a-n/a.

715 MONERIE, P. A., M. BIASUTTI and P. ROUCOU. 2016. On the projected increase of Sahel rainfall during the
716 late rainy season. *International Journal of Climatology*, **36**(13), pp.4373-4383.

717 NGATCHA, B. N. 2009. Water resources protection in the Lake Chad Basin in the changing environment.
718 *European Water*, **25**(26), pp.3-12.

719 NICHOLSON, S. E. 2009. A revised picture of the structure of the “monsoon” and land ITCZ over West Africa.
720 *Climate dynamics*, **32**(7-8), pp.1155-1171.

721 NICHOLSON, S. E. 2013. The West African Sahel: A review of recent studies on the rainfall regime and its
722 interannual variability. *ISRN Meteorology*, **2013**.

723 NICHOLSON, S. E. 2018. The ITCZ and the Seasonal Cycle over Equatorial Africa. *Bulletin of the American*
724 *Meteorological Society*, **99**(2), pp.337-348.

725 NKIAKA, E., N. NAWAZ and J. C. LOVETT. 2017a. Evaluating Global Reanalysis Datasets as Input for
726 Hydrological Modelling in the Sudano-Sahel Region. *Hydrology*, **4**(1), p13.

727 NKIAKA, E., N. R. NAWAZ and J. C. LOVETT. 2017b. Analysis of rainfall variability in the Logone catchment,
728 Lake Chad basin. *International Journal of Climatology*, **37**(9), pp.3553-3564.

729 NKIAKA, E., N. R. NAWAZ and J. C. LOVETT. 2017c. Effect of single and multi-site calibration techniques on
730 hydrological model performance, parameter estimation and predictive uncertainty: a case study in
731 the Logone catchment, Lake Chad basin. *Stochastic environmental research and risk assessment*,
732 10.1007/s00477-017-1466-0.

733 OCHA. 2017. *Lake Chad Basin: Crisis Update*

734 ODADA, E., L. OYEBANDE and J. OGUNTOLA. 2009. *Lake Chad experience and lessons learned*.

735 OKPARA, U. T., L. C. STRINGER, A. J. DOUGILL and M. D. BILA. 2015. Conflicts about water in Lake Chad: Are
736 environmental, vulnerability and security issues linked? *Progress in Development Studies*, **15**(4),
737 pp.308-325.

738 PARK, J.-Y., J. BADER and D. MATEI. 2015. Northern-hemispheric differential warming is the key to
739 understanding the discrepancies in the projected Sahel rainfall. *Nature communications*, **6**.

740 PATTNAYAK, K., S. KAR, M. DALAL and R. PATTNAYAK. 2017. Projections of annual rainfall and surface
741 temperature from CMIP5 models over the BIMSTEC countries. *Global and Planetary Change*, **152**,
742 pp.152-166.

743 PEEL, M. C., B. L. FINLAYSON and T. A. MCMAHON. 2007. Updated world map of the Köppen-Geiger climate
744 classification. *Hydrol. Earth Syst. Sci.*, **11**(5), pp.1633-1644.

745 POLSON, D., M. BOLLASINA, G. HEGERL and L. WILCOX. 2014. Decreased monsoon precipitation in the
746 Northern Hemisphere due to anthropogenic aerosols. *Geophysical Research Letters*, **41**(16),
747 pp.6023-6029.

- 748 QUESADA, B., N. DEVARAJU, N. DE NOBLET-DUCOUDRÉ and A. ARNETH. 2017. Reduction of monsoon rainfall
749 in response to past and future land use and land cover changes. *Geophysical Research Letters*, **44**(2),
750 pp.1041-1050.
- 751 RAWLINS, M., R. S. BRADLEY and H. DIAZ. 2012. Assessment of regional climate model simulation estimates
752 over the northeast United States. *Journal of Geophysical Research: Atmospheres*, **117**(D23).
- 753 ROWELL, D. P. 2013. Simulating SST teleconnections to Africa: What is the state of the art? *Journal of*
754 *Climate*, **26**(15), pp.5397-5418.
- 755 SCHEWE, J., J. HEINKE, D. GERTEN, I. HADDELAND, N. W. ARNELL, D. B. CLARK, R. DANKERS, S. EISNER, B. M.
756 FEKETE and F. J. COLÓN-GONZÁLEZ. 2014. Multimodel assessment of water scarcity under climate
757 change. *Proceedings of the National Academy of Sciences*, **111**(9), pp.3245-3250.
- 758 SENGUPTA, A. and M. RAJEEVAN. 2013. Uncertainty quantification and reliability analysis of CMIP5
759 projections for the Indian summer monsoon. *Current Science*, pp.1692-1703.
- 760 SIAM, M. S., M.-E. DEMORY and E. A. B. ELTAHIR. 2013. Hydrological Cycles over the Congo and Upper Blue
761 Nile Basins: Evaluation of General Circulation Model Simulations and Reanalysis Products. *Journal*
762 *of Climate*, **26**(22), pp.8881-8894.
- 763 TANVEER, M. E., M.-H. LEE and D.-H. BAE. 2016. Uncertainty and Reliability Analysis of CMIP5 Climate
764 Projections in South Korea Using REA Method. *Procedia Engineering*, **154**, pp.650-655.
- 765 TAYLOR, C. M., D. BELUŠIĆ, F. GUICHARD, D. J. PARKER, T. VISCHEL, O. BOCK, P. P. HARRIS, S. JANICOT, C.
766 KLEIN and G. PANTHOU. 2017. Frequency of extreme Sahelian storms tripled since 1982 in satellite
767 observations. *Nature*, **544**(7651), pp.475-478.
- 768 TAYLOR, K. E., R. J. STOUFFER and G. A. MEEHL. 2012. An overview of CMIP5 and the experiment design.
769 *Bulletin of the American Meteorological Society*, **93**(4), pp.485-498.
- 770 TEBALDI, C. and R. KNUTTI. 2007. The use of the multi-model ensemble in probabilistic climate projections.
771 *Philosophical Transactions of the Royal Society of London A: Mathematical, Physical and Engineering*
772 *Sciences*, **365**(1857), pp.2053-2075.
- 773 TRENBERTH, K. E. 2011. Changes in precipitation with climate change. *Climate Research*, **47**(1-2), pp.123-
774 138.
- 775 WASHINGTON, R., M. C. TODD, S. ENGELSTAEDTER, S. MBAINAYEL and F. MITCHELL. 2006. Dust and the low-
776 level circulation over the Bodélé Depression, Chad: Observations from BoDEx 2005. *Journal of*
777 *Geophysical Research: Atmospheres*, **111**(D3).
- 778 WEEDON, G. P., G. BALSAMO, N. BELLOUIN, S. GOMES, M. J. BEST and P. VITERBO. 2014. The WFDEI
779 meteorological forcing data set: WATCH Forcing Data methodology applied to ERA-Interim
780 reanalysis data. *Water Resources Research*, **50**(9), pp.7505-7514.
- 781 WEHNER, M. 2013. Methods of Projecting Future Changes in Extremes. In: A. AGHAKOUCHAK, D.
782 EASTERLING, K. HSU, S. SCHUBERT and S. SOROOSHIAN, eds. *Extremes in a Changing Climate:*
783 *Detection, Analysis and Uncertainty*. Dordrecht: Springer Netherlands, pp.223-237.
- 784 WOLDEMESKEL, F., A. SHARMA, B. SIVAKUMAR and R. MEHROTRA. 2012. An error estimation method for
785 precipitation and temperature projections for future climates. *Journal of Geophysical Research:*
786 *Atmospheres*, **117**(D22).

787

788